A New Type of Efficient CO_2 Adsorbent with Improved Thermal Stability: Self-Assembled Nanohybrids with Optimized Microporosity and Gas Adsorption Functions

*Tae Woo Kim, In Young Kim, Tae Sung Jung, Chang Hyun Ko, and Seong-Ju Hwang**

A new type of efficient CO_2 absorbent with improved thermal stability is synthesized via self-assembly between 2D inorganic nanosheets and two kinds of 0D inorganic nanoclusters. In these self-assembled nanohybrids, the nanoclusters of CdO and Cr_2O_3 are commonly interstratified with layered titanate nanosheets, leading to the formation of highly microporous pillared structure with increased basicity of pore wall. The co-pillaring of basic CdO with Cr_2O_3 is fairly effective at increasing a proportion of micropores and reactivity for CO_2 molecules and at improving the thermal stability of the resulting porous structure. Of prime importance is that the present inorganic-pillared nanohybrids show highly efficient CO_2 adsorption capacity, which is much superior to those of many other absorbents and compatible to those of CO_2 adsorbing metal–organic framework (MOF) compounds. Taking into account an excellent thermal stability of the present nanohybrids, these materials are very promising CO_2 adsorbents usable at elevated temperature. This is the first example of efficient CO_2 adsorbent from pillared materials. The co-pillaring of basic metal oxide nanoclusters employed in this study can provide a very powerful way of developing thermally stable CO_2 adsorbents from many known pillared systems.

1. Introduction

A great deal of research effort is devoted for the synthesis of porous inorganic solids and their application for the capturing of greenhouse gas and the storage of gaseous fuel.[1–4] The sequestration of CO_2 gas is one of the most important issues in mitigating increasing threats of global warming.[1,5–8] There are several factors for an optimization of the gas absorption function of porous materials such as high proportion of micropores, high reactivity for gas molecules, and readily accessible pore structure.[1–8] Diverse porous materials such as zeolite-related materials and metal–organic framework (MOF) are applied as CO_2 gas adsorbents.[5–14] Zeolite-related materials show well-defined microporous structure but have several drawbacks including a low reactivity for CO_2 molecules and a difficulty in controlling the size and chemical nature of pores.[12–14] MOF boasts well-ordered microporous structure and highly expanded surface area but the low thermal and chemical stability of this material limits its use as gas adsorbent at harsh condition.[2,5–11] Thus it is highly desirable to synthesize thermally stable porous materials with excellent gas adsorption functions. Alternatively, the pillaring of guest species into layered materials via ion-exchange reaction can provide another route to porous materials.[15–20] Although the inorganic-pillared materials possess much better thermal stability than do MOFs, they also suffer from a broad distribution of pore size and a low reactivity for CO_2 molecule. To dates, there is no inorganic-pillared material showing efficient CO_2 adsorption capability and high thermal stability. In addition to conventional ion-exchange method, a self-assembly between exfoliated inorganic nanosheets and nanosized inorganic guest species can provide an alternative way to synthesize highly porous pillared nanohybrids with improved thermal stability.[21–23] The resulting self-assembled materials show remarkably expanded surface area and high porosity, thus being applicable as gas adsorbents. In comparison with the ion-exchange route, this self-assembly method using 2D nanosheets and 0D nanoclusters possesses much greater flexibility in material design, that is, a facile control of pore size, chemical bonding nature of pore walls, and thermal stability of pillared structure via the tuning of the composition and structure of component nanostructures. The adsorption capability of the resulting pillared material for CO_2 molecules having acidic nature might be enhanced by an increase of the basicity of pore walls as well as by the tailoring of pore diameter to micropore-level.[1–8,24,25] Yet we are aware of no report not only on the development of efficient CO_2 adsorbents from

Dr. T. W. Kim, I. Y. Kim, Prof. S.-J. Hwang
Center for Intelligent Nano-Bio Materials (CINBM)
Department of Chemistry and Nano Sciences
Ewha Womans University
Seoul 120-750, Korea
E-mail: hwangsju@ewha.ac.kr
Dr. T. S. Jung
Clean Fuel Research Center
Korea Institute of Energy Research
Daejon 305-343, Korea
Prof. C. H. Ko
School of Applied Chemical Engineering
Chonnam National University
Gwangju 500-757, Korea

DOI: 10.1002/adfm.201300071

pillared materials but also on the control of the gas adsorption function of pillared materials via the co-pillaring of nanoclusters with basic nature.

In the present study, microporous pillared nanohybrids with improved gas adsorption function can be synthesized by a self-assembly between layered titanate nanosheets and two kinds of Cr_2O_3/CdO nanoclusters. The co-pillaring of basic cadmium oxide with chromium oxide provides a new methodology to synthesize highly efficient CO_2 adsorbents with improved thermal stability.

2. Results and Discussion

2.1. Powder XRD Analysis

The powder X-ray diffraction (XRD) patterns of the as-prepared Cr_2O_3/CdO–layered titanate nanohybrids with different Cd/Cr ratios of 1/9, 2/8, 3/7, and 4/6 (hereafter these materials are denoted as **CCT1**, **CCT2**, **CCT3**, and **CCT4**) are presented in the left panel of **Figure 1**, together with those of the protonated titanate and Cd-free Cr_2O_3–layered titanate nanohybrid synthesized by the same self-assembly method (hereafter this material is denoted as **CT**). Except **CCT4** showing X-ray amorphous structure, all of the as-prepared nanohybrids exhibit a series of (*0k0*) reflections at lower 2θ region compared to the protonated titanate, indicating the formation of well-ordered intercalation structure accommodating nanosized metal oxide clusters.[21–23] The (*0k0*) reflections of the as-prepared **CCT1**, **CCT2**, and **CCT3** appear at lower angle than that of Cd-free **CT** nanohybrid, suggestive of additional basal increment induced by the co-intercalation of cadmium oxide nanocluster with chromium oxide nanocluster. From the least-squares fitting analysis, the basal spacings of the nanohybrids are determined as 25.1, 27.7, and 31.3 Å for **CCT1**, **CCT2**, and **CCT3**, respectively, which correspond to the gallery heights of 18.1, 20.7, and 24.3 Å. The estimated basal spacings of the co-pillared **CCT** nanohybrids are much greater than that of the unpillared layered titanate without Cr_2O_3/CdO nanoclusters (d = 9.4 Å; see Supporting Information), clearly demonstrating the usefulness of co-pillaring in expanding the interlayer space of layered titanate. Also all the present **CCT** nanohybrids have larger basal spacing compared with the Cd-free **CT** (d = 21.7 Å) nanohybrid,[21] confirming the co-intercalation of cadmium species with chromium one. A gradual increase of basal spacing with increasing Cd content clearly demonstrates that the co-intercalation of two kinds of nanoclusters allows us to control the crystal structure of the pillared nanohybrids. In contrast to the intercalation of Cr_2O_3 nanocluster, that of CdO nanocluster cannot be achieved without a co-intercalant of Cr_2O_3. Generally the hydrolysis of the Cd^{2+} ion occurs above pH = 7 in concentrated solution. In highly basic condition like the colloidal suspension of layered titanate nanosheets (pH > 12), cadmium ion exists as negatively charged $Cd(OH)_4^{2-}$ cluster.[26] Since the exfoliated nanosheets of layered titanate possess negative surface charge, the negatively charged cadmium hydroxide cluster ions cannot be hybridized with negatively charged titanate nanosheets. Conversely, in the given pH condition, chromium ion forms cationic polyoxonuclear chromium hydroxide clusters.[26] Thus it can be readily hybridized with oppositely charged titanate nanosheets. In terms of an electrostatic attraction with chromium hydroxide clusters, the negatively charged cadmium cluster can be co-intercalated into the layered titanate lattice, leading to the formation of the co-pillared Cr_2O_3/CdO–layered titanate nanohybrid. As plotted in Figure 1, some weak impurity peaks are observed for the nanohybrids with higher Cd/Cr ratios (**CCT2**, **CCT3**, and **CCT4**) whereas the as-prepared **CCT1** nanohybrid does not show any peak corresponding to unpillared Cr_2O_3 or CdO phase (see Supporting Information). Because of the occupation of gallery space by too high content of co-intercalated CdO species and/or the formation of non-porous impurity phase, the nanohybrids with higher Cd/Cr ratios (**CCT2**, **CCT3**,

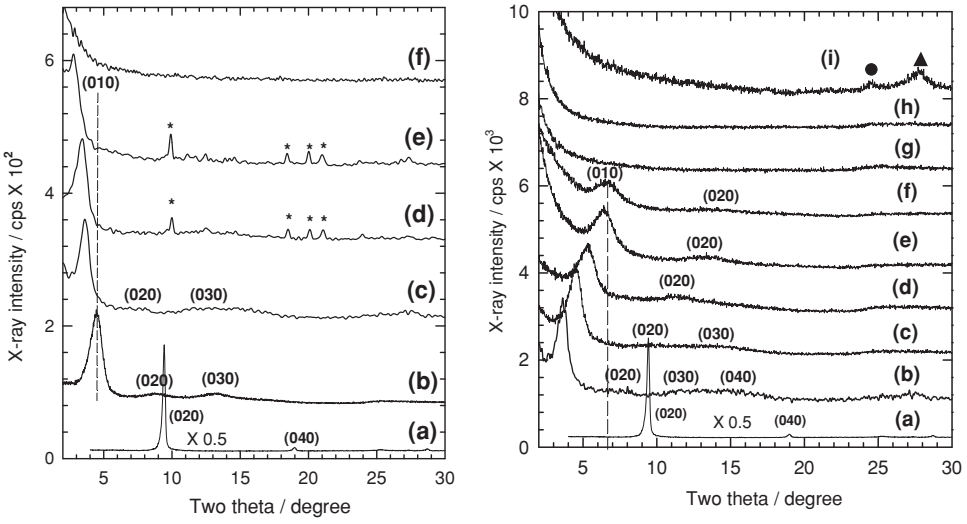

Figure 1. Left: powder XRD patterns of a) the protonated titanate and b) **CT**, c) **CCT1**, d) **CCT2**, e) **CCT3**, and f) **CCT4** nanohybrids. Right: powder XRD patterns of a) the protonated titanate, b) **CCT1** and its derivatives calcined at c) 200, d) 300, e) 400, f) 500, g) 600, h) 700, and i) 800 °C. The asterisks, circle, and triangle indicate the Bragg reflections of Cd-related impurity phase, Cr_2O_3, and rutile TiO_2, respectively.

and **CCT4**) display smaller surface area and poorer CO_2 adsorption capability than does the **CCT1** nanohybrid (see Supporting Information). Thus, further investigations are carried out for the single-phase compound of **CCT1**.

2.2. FE-SEM, HR-TEM, and Elemental Analysis

The crystal morphology of the as-synthesized **CCT1** nanohybrid is monitored with field emission-scanning electron microscopy (FE-SEM). As shown in **Figure 2**a, this material exhibits the well-ordered stacking of layered titanate nanosheets with quite thin thickness. This underscores the fact that the layered titanate sheets and guest oxide particles in this material are assembled in a layer-by-layer fashion, as illustrated in Figure 2b. Such an interstratified structure of this material is also confirmed by the cross-sectional high-resolution transmission electron microscopy (HR-TEM) image in Figure 2c. A cross-sectional view of as-prepared **CCT1** nanohybrid shows an assembly of well-developed parallel dark stripes. Such parallel dark lines correspond to layered titanate lattice. This clearly demonstrates the formation of a heterostructure between layered titanate and guest oxide nanoparticles. In contrast to the host lattice, the intercalated guest nanoclusters of Cr_2O_3/CdO are not clearly observable in the present cross-sectional HR-TEM image, which is attributable to their lower electron density than the host layered titanate layers. This is common for most of cross-sectional HR-TEM results for the pillared metal oxides.[21,22] From the distance between titanium oxide layers, the basal spacing of this nanohybrid is determined as ≈25 Å, which is well-consistent with the *b*-axis lattice parameter obtained from powder XRD analysis. The contents of Ti, Cr, and Cd elements in the present **CCT1** nanohybrid are determined by performing ICP and EDS (see Supporting Information). According to two spectrometric analyses, the **CCT1** nanohybrid contains Ti, Cr, and Cd ions with the ratios of (Cr+Cd)/Ti = 0.64 and Cr/Cd = 6.19, confirming the co-intercalation of CdO and Cr_2O_3.

2.3. Structural Variation of the CCT1 upon Heat-Treatment

The evolution of the pillared structure of **CCT1** upon heat-treatment is probed with powder XRD. As plotted in the right panel of Figure 1, the heat-treatment at elevated temperatures gives rise to a high-angle shift of (*0k0*) reflections, indicative of the pillaring of guest species with a partial shrinkage of basal spacing. The observed lattice contraction is attributable to the densification of guest cluster species with dehydroxylation and/or to the dehydration of **CCT1** (see Supporting Information). The pillared structure of **CCT1** is well-maintained up to 500 °C. This material shows better thermal stability than **CT** showing a collapse of pillared structure at 500 °C.[21] The present findings provide strong evidence for the usefulness of the co-pillaring of CdO and Cr_2O_3 nanoclusters in enhancing the thermal stability of pillared structure. Such an improvement of the thermal stability of co-pillared material is attributable to the formation of the multistacked structure of two kinds of inorganic nanoclusters in the interlayer space of host lattice, as reported for the SiO_2/TiO_2-pillared clays.[27] After the calcination at 600 and 700 °C, this **CCT1** material displays no distinct Bragg XRD peaks, reflecting the collapse of pillared structure. A close inspection on the high angle XRD data reveals that the

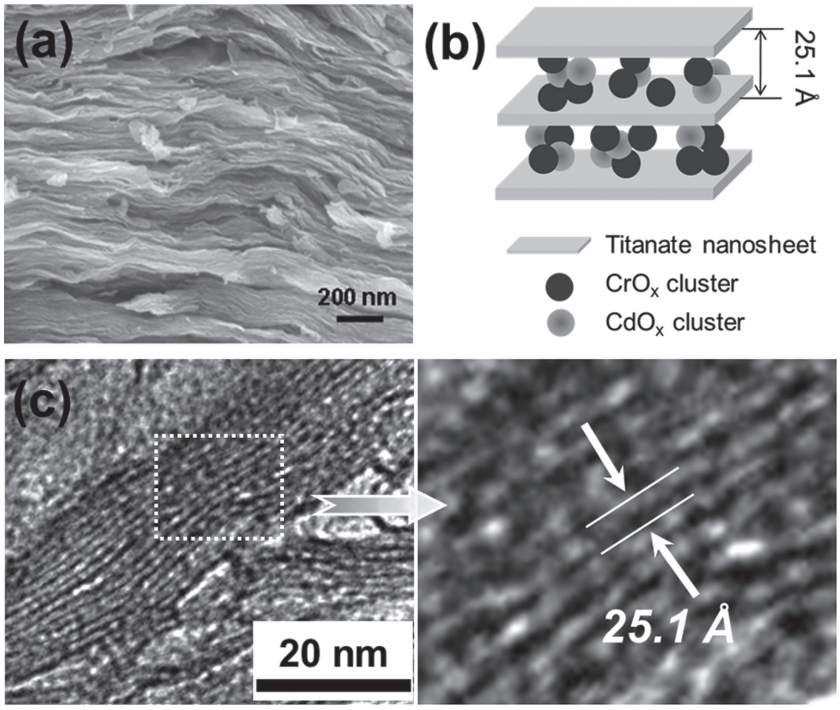

Figure 2. a) FE-SEM, b) schematic model, and c) cross-sectional HR-TEM images for the as-prepared **CCT1** nanohybrid.

CCT1 nanohybrids calcined at ≤700 °C do not show any impurity peaks related to unpillared Cr_2O_3 or CdO phase (see Supporting Information). Conversely, the heat-treatment at 800 °C induces the formation of rutile TiO_2 and Cr_2O_3 phases, indicating the complete destruction of pillared structure (see Supporting Information).

2.4. X-Ray Absorption Spectroscopy

The local atomic arrangement and electronic structure of the titanium ion in the as-prepared **CCT1** material and its derivatives calcined at 200 – 800 °C are examined with Ti K-edge X-ray absorption near-edge structure (XANES) spectroscopy. As plotted in **Figure 3**, all of the materials under investigation display pre-edge peaks P_1, P_2, and P_3 corresponding to the 1s → 3d transitions as well as several main-edge peaks A, B, and C related to the 1s → 4p transitions.[28] The as-prepared **CCT1** material and its derivatives calcined at 200–700 °C commonly show nearly identical spectral features to the pristine layered titanate in the both pre-edge and main-edge regions. This result indicates the maintenance of lepidocrocite-type layered titanate lattice upon the hybridization with Cr_2O_3/CdO and the following heat-treatment at 200–700 °C.[29] Although the heat-treatment at 600–700 °C causes the collapse of pillared structure, the present XANES result indicates the retention of the layer-type local structure of titanate component. Conversely, the **CCT1** material calcined at 800 °C demonstrates significant spectral change to a rutile TiO_2-like feature, providing clear evidence for the phase transformation of layered titanate to rutile TiO_2.

Also the electronic structure and local atomic arrangement of chromium and cadmium ions in the as-prepared **CCT1** nanohybrid and its derivatives calcined at 200–800 °C are studied with XANES spectroscopy at Cr K- and Cd K-edge. As shown in the Cr K-edge XANES spectra in the left panel of **Figure 4**, all of the present materials exhibit pre-edge peak P corresponding to the 1s → 3d transition. The position of the peak P appears almost identical for all the **CCT1** nanohybrids and reference Cr_2O_3, indicating the trivalent oxidation state of chromium ions in the present nanohybrid materials.[30] As can be seen clearly from the middle panel of Figure 4, the weak intensity of the peak P allows us to rule out the possibility of a hexavalent chromium ion in the **CCT1** nanohybrids. After the heat-treatment at ≥300 °C, another pre-edge peak P′, a fingerprint for the Cr_2O_3 phase, appears for the **CCT1** nanohybrid, suggesting the structural change to Cr_2O_3-like local atomic arrangement.[21] The formation of Cr_2O_3-like local structure upon the calcination at elevated temperature is further confirmed by the appearance of main-edge feature A. The right panel of Figure 4 represents the Cd K-edge XANES spectra for the as-prepared **CCT1** and its calcined derivatives, together with that for the reference CdO. The as-prepared **CCT1** material displays high spectral similarity in terms of edge energy and overall spectral feature to the reference CdO, indicating the divalent Cd oxidation state and CdO-type local structure of

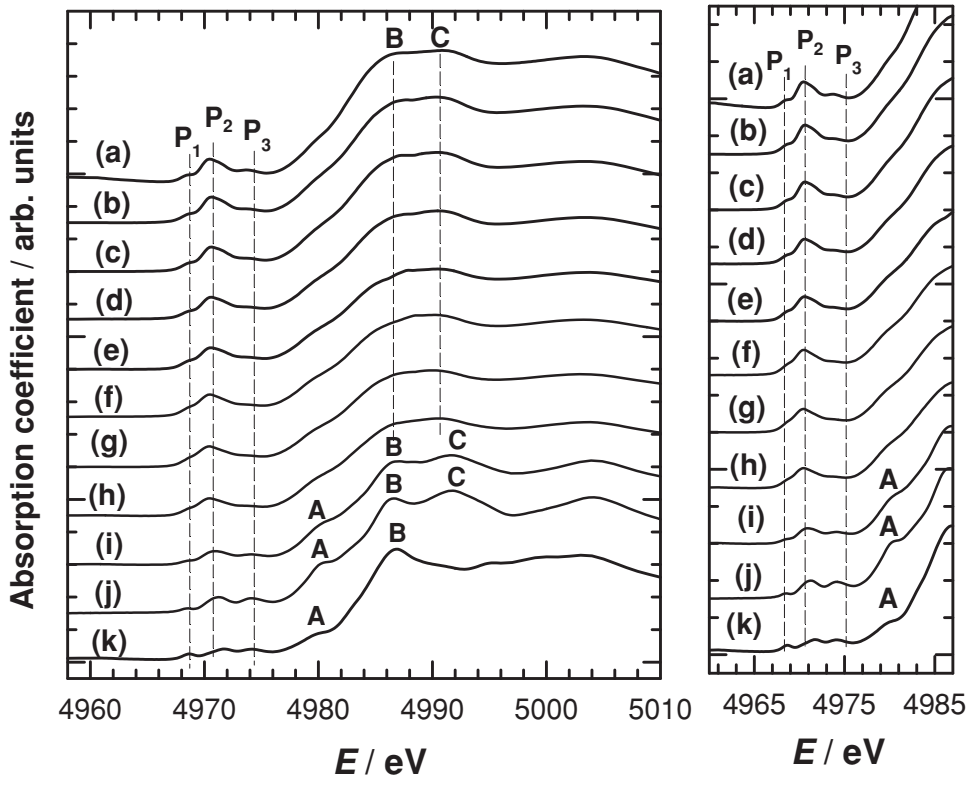

Figure 3. Ti K-edge XANES spectra for a) the pristine layered titanate, b) the as-prepared **CCT1** nanohybrid and its derivatives calcined at c) 200, d) 300, e) 400, f) 500, g) 600, h) 700, and i) 800 °C, together with the references of j) rutile TiO_2 and k) anatase TiO_2. The enlarged pre-edge spectra in the range of 4962–4986 eV are presented in the right panel.

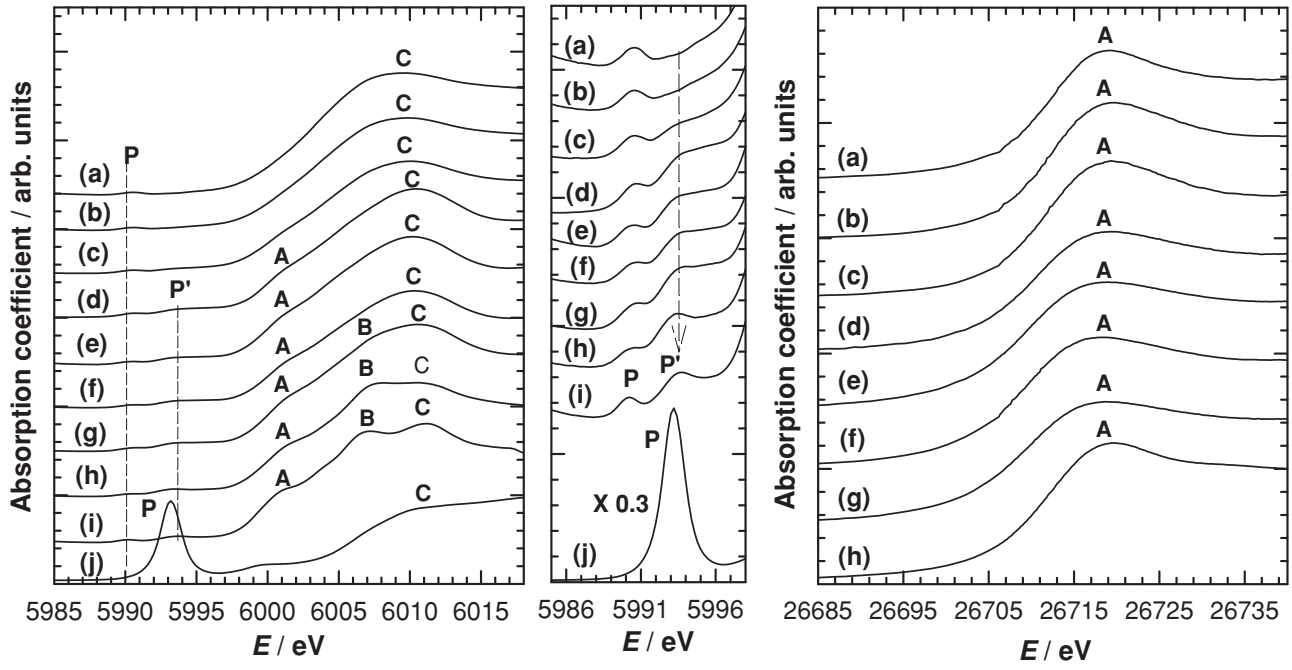

Figure 4. Left: Cr K- and right: Cd K-edge XANES spectra for a) the as-prepared **CCT1** nanohybrid and its derivatives calcined at b) 200, c) 300, d) 400, e) 500, f) 600, g) 700, h) 800°C/CdO, i) Cr_2O_3 and j) Na_2CrO_4, respectively. The enlarged pre-edge Cr K-edge XANES spectra in the range of 5985–5998 eV are presented in the middle panel.

co-pillared cadmium species. The calcination at elevated temperatures has negligible influence on the spectral feature of **CCT1** nanohybrid, indicating the maintenance of CdO-type structure upon the heat-treatment. The local structure of co-intercalated cadmium species in the as-prepared and calcined **CCT1** materials is probed with Cd K-edge EXAFS analysis (see Supporting Information). The Cd K-edge k^3-weighted EXAFS spectra and the corresponding Fourier transforms (FTs) of the as-prepared **CCT1** material and its calcined derivative at 500 °C are quite similar to those of bulk CdO. This finding demonstrates the rocksalt CdO-type local structure of co-pillared species. A close inspection on the FT data reveals that the **CCT1** nanohybrids show lower FT intensity than that does the bulk CdO reference, indicating the nanocrystalline nature of co-intercalated CdO species.

2.5. N_2 Adsorption–Desorption Isotherm Measurement

The pore structure and gas adsorption property of the **CCT1** nanohybrids are investigated with N_2 adsorption–desorption isotherm analysis. As plotted in **Figure 5**a, all of the nanohybrids except for 800 °C-calcined sample exhibit the BDDT type I and IV shape of isotherms, along with H3-type hysteresis loop in the IUPAC classification.[31] This suggests the generation of open slit-shaped capillaries with very wide bodies and narrow short necks. The as-prepared **CCT1** and its calcined derivatives commonly display strong N_2 adsorption at $pp_0^{-1} < 0.05$, indicating the presence of a high concentration of micropores. As summarized in **Table 1**, the fitting analysis to BET equation demonstrates that all the present nanohybrids possess remarkably expanded surface areas of ≈100–191 m^2 g^{-1}, which are much larger than that of the pristine layered titanate (≈1 m^2 g^{-1}). This indicates the usefulness of the self-assembly between nanosheets and nanoclusters in forming highly porous structure. Among the present **CCT1** nanohybrids, the calcined derivative at 500 °C possesses the largest surface area (S_{BET}: 191 m^2 g^{-1}, $S_{Langmuir}$: 287 m^2 g^{-1}). To evaluate the microporosity of as-prepared **CCT1** and its calcined derivatives, a de Boer's *t*-plot analysis is carried out using the adsorption branch.[31] As listed in Table 1, the *t*-plot analysis clearly demonstrates the predominant existence of micropores in the pillared materials. In particular, the **CCT1** calcined at 500 °C exhibits the largest microporous surface area of 155 m^2 g^{-1} (≈81% of the total surface area), which is much greater than that of **CT** (S_{micro}: 91 m^2 g^{-1}) calcined at the same temperature (Table 1). This finding clearly demonstrates that the co-pillaring of CdO and Cr_2O_3 markedly increases the proportion of micropores. Such a change in pore structure is attributable to the tight packing of two kinds of guest metal oxides, resulting in the uniform and stable pillared structure with micropores. According to pore size distribution calculation based on the MP method using adsorption branch of BET isotherm in Figure 5b,[31] the as-prepared **CCT1** and its derivatives calcined up to 500 °C display a narrow micropore range of 6–14 Å with a slit width (≈10 Å, estimated by the *t*-plot method). Such a slit width of <10 Å corresponds to gallery space in the present pillared nanohybrids (see Supporting Information), which is consistent with the basal spacings determined from XRD and HR-TEM results.

2.6. Adsorption Tests for Carbon Dioxide and Hydrogen Gases

The gas adsorption functions of the present nanohybrid materials are tested for greenhouse CO_2 gas. As plotted in **Figure 6**,

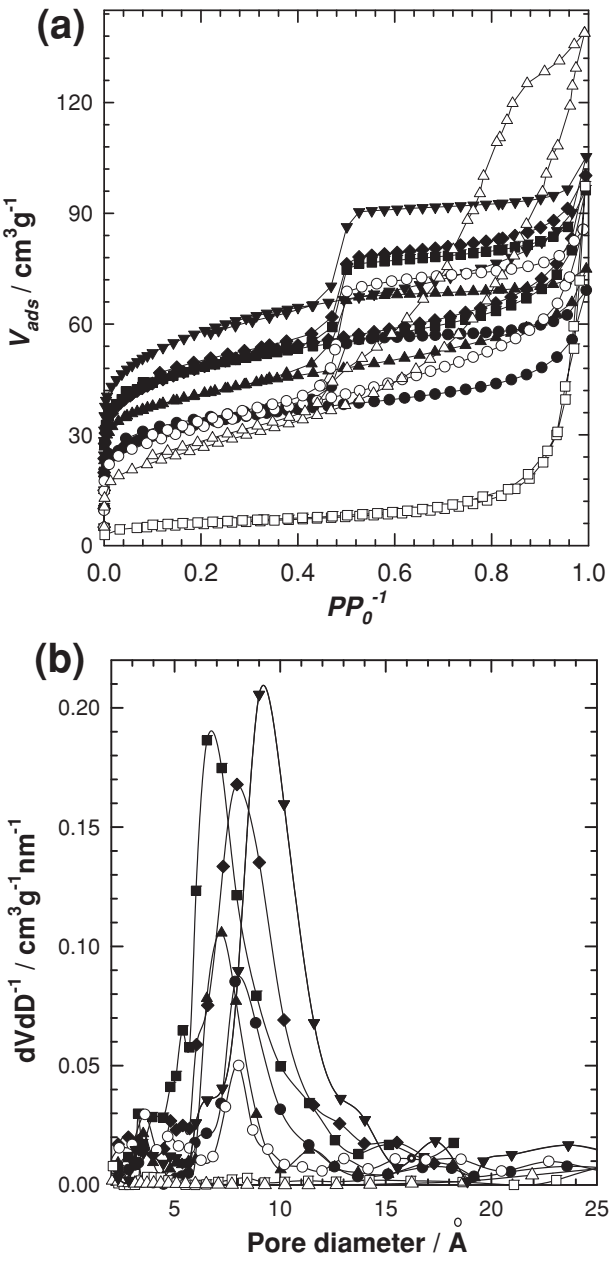

Figure 5. a) N_2 adsorption–desorption isotherms and b) the micropore size distribution calculated on the basis of the MP-method for the as-prepared **CCT1** nanohybrid and its derivatives calcined at 200 (▲), 300 (■), 400 (✦), 500 (▼), 600 (○), 700 (△), and 800 °C (□).

the as-prepared **CCT1** nanohybrid shows promising functionality as CO_2 adsorbent, which is further improved by heat-treatment at elevated temperature. Even after heat-treatment at 700 °C, the **CCT1** nanohybrid can adsorb a distinct amount of CO_2 gas, indicating its excellent thermal stability. At 0 °C and 101.325 kPa (standard temperature and pressure, or STP), the most efficient adsorption of CO_2 molecules occurs for the **CCT1** calcined at 500 °C (40.0 cm^3 g^{-1} STP or 1.78 mmol g^{-1}). The observed adsorption capacity of this material is markedly superior to that of **CT** calcined at the same temperature (12.6 cm^3 g^{-1} STP, 0.56 mmol g^{-1}). The CO_2 adsorption ability of the **CCT1** material calcined at 500 °C is even greater than that of the **CT** calcined at 400 °C (28.0 cm^3 g^{-1} STP, 1.25 mmol g^{-1}) having a larger surface area (S_{BET}: 228 m^2 g^{-1}), underscoring the validity of co-pillaring method in improving CO_2 adsorption functionality. Additional CO_2 adsorption tests are carried out for the **CCT1** calcined at 500 °C under the condition of room temperature (25 °C) and 101.325 kPa. Under this condition, this material still retains a promising CO_2 adsorption performance (21.1 cm^3 g^{-1} STP or 0.94 mmol g^{-1}) with a good reproducibility (see Supporting Information). Although the adsorption capacity of the **CCT1** calcined at 500 °C is somewhat decreased with the increase of measurement temperature from 0 °C to 25 °C, the degree of adsorption reduction is weaker or similar to those of other CO_2 adsorbent materials.[5–16] Also, the multiple cycling performance of CO_2 adsorption is tested for the 500 °C-calcined **CCT1** (see Supporting Information). This material does not show any marked decrease of its CO_2 adsorption capability for four repeated cycles at both 0 and 25 °C. This result allows us to verify the usefulness of the present **CCT1** nanohybrid as a recyclable CO_2 adsorbent.

The **CCT1** nanohybrid calcined at 500 °C showing the highest activity for CO_2 adsorption is also tested as H_2 adsorbent (see Supporting Information). At –196 °C and 101.325 kPa, the derivative of **CCT1** material calcined at 500 °C shows an effective adsorption of H_2 gas with the adsorption volume of 45.7 cm^3 g^{-1} STP or 2.04 mmol g^{-1}. The observed adsorption capability of the pillared **CCT1** nanohybrid is comparable to those of many known and efficient H_2 adsorbents.[2,19,32–37] This result strongly suggests that the present **CCT1** nanohybrid is also applicable for the storage of H_2 gas. The **CCT1** nanohybrid shows BDDT type I shape of H_2 adsorption isotherm with a steep rise at very low pressure, indicating the interpenetration of H_2 into the micropores. This result strongly suggests that the adsorption of gas molecules occurs in the micropores of the present nanohybrid materials. To confirm the beneficial effect of the co-pillaring on the gas adsorption function of metal oxide, the CO_2 and H_2 adsorption abilities of the non-pillared mixture of Cr_2O_3 and CdO with the Cr/Cd molar ratio of 6.19 are tested. Under the condition of 0 °C and 101.325 kPa, this material exhibits much poorer adsorption capacity of CO_2 molecules (0.73 cm^3 g^{-1} STP or 0.034 mmol g^{-1}) and H_2 molecules (0.5 cm^3 g^{-1} STP or 0.02 mmol g^{-1} at –196 °C, 101.325 kPa) than does the **CCT1** nanohybrid calcined at 500 °C (see Figure 6 and Supporting Information). This observation clearly demonstrates that the formation of pillared structure is of crucial importance in achieving the good adsorption functions of the present **CCT** nanohybrids. The observed enhancement of CO_2 adsorption capacity upon the co-pillaring can be understood by the following factors; the first factor is an increase of reactivity for acidic CO_2 molecules via the co-incorporation of basic CdO nanoclusters. The heavier metal oxide with lower metal oxidation state like CdO has a higher basicity than the lighter metal oxide with higher metal oxidation state like Cr_2O_3, which is advantageous for the adsorption of CO_2 molecules with acidic nature.[38–40] This supposition is supported by the experimental finding that the **CCT1** calcined at 500 °C with smaller surface area displays a greater CO_2 adsorption capability than the CdO-free **CT** calcined at 400 °C with larger surface area. The crucial role of basic Cd ions is further confirmed by the previous reports showing the higher

Table 1. Specific surface area and pore parameters of the **CCT1** nanohybrids, the pristine layered titanates, and Cd-free **CT** nanohybrids determined from N_2 adsorption–desorption measurements.

	Specific surface area					
Sample	S_{BET} (m^2 g^{-1})	$S_{Langmuir}$ (m^2 g^{-1})	S_{micro}(m^2 g^{-1})	Slit width[a)] (Å)	V_t[b)] (mL g^{-1} STP)	V_m[c)] (mL g^{-1} STP)
Cesium titanate	≈1	≈1	–	–	–	–
Protonated titanate	≈10	≈17	–	–	–	–
CT-500 °C	126 (0.9999)	166 (0.9983)	91	8.6	0.1185	0.0456
CCT1-RT	109 (0.9988)	162 (0.9993)	89	7.8	0.1070	0.0465
CCT1-200 °C	134 (0.9991)	200 (0.9992)	105	6.8	0.1159	0.0567
CCT1-300 °C	157 (0.9987)	234 (0.9995)	126	7.0	0.1489	0.0667
CCT1-400 °C	160 (0.9988)	237 (0.9993)	127	7.6	0.1550	0.0668
CCT1-500 °C	191 (0.9988)	287 (0.9993)	155	8.5	0.1630	0.0804
CCT1-600 °C	110 (0.9995)	168 (0.9968)	65	8.0	0.1324	0.0366
CCT1-700 °C	94 (0.9999)	148 (0.9952)	–	–	0.2147	–
CCT1-800 °C	20 (0.9997)	31 (0.9957)	–	–	0.1111	–

[a)]The slit widths are estimated by the *t*-plot method; [b)]V_t = total pore volume; [c)]V_m = micropore volume (estimated by the *t*-plot). The digits in parenthesis denote correlation factors.

CO_2 adsorption capability of Cd based-MOFs than 3d transition metal (*M* = Mn, Co, Zn) based-MOF.[41–42] Second, the optimized micropore structure of the **CCT1** materials is fairly beneficial for efficient diffusion of CO_2 gas. There are many reports about the higher activity of micropores to adsorb gas molecules compared with larger mesopores or macropores.[43–45] Third, the incorporation of nanocrystalline metal oxides in-between layered titanate nanosheets leads to the exposure of many metal sites in micropore wall available for the adsorption of gas molecules. As a consequence of these factors, the CO_2 adsorption capacity of the present **CCT1** calcined at 500 °C is superior to those of any other pillared materials and many other adsorbents.[1–17,32–36,46–47] The observed CO_2 adsorption capacity of this material is comparable to those of MOFs, even though the MOFs possess much larger surface area than the **CCT1**.[32–34,36] This fact underscores the merit of the pillaring of basic nanocluster. An excellent thermal stability and a high adsorption capability of **CCT1** render this material very promising CO_2 adsorbent.

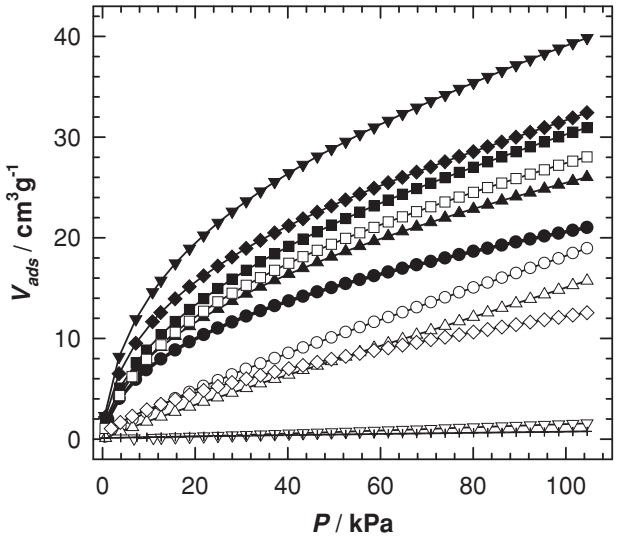

Figure 6. The CO_2 adsorption behaviors of the as-prepared **CCT1** nanohybrid (●)and its derivatives calcined at 200 (▲), 300 (■), 400 (✦), 500 (▼), 600 (○), and 700 °C (△), the protonated layered titanate (▽), the **CT** nanohybrids calcined at 400 (□) and 500 °C (◊), and the non-pillared mixture of Cr_2O_3 and CdO (+). All the present data are measured at 0 °C up to 101.325 kPa.

3. Conclusion

In conclusion, a novel lattice engineering method to synthesize efficient CO_2 adsorbents from pillared system is developed on the basis of the self-assembly of basic metal oxide nanoclusters with 2D nanosheets. The intercalative hybridization of basic CdO with Cr_2O_3 provides a powerful way of improving the microporosity, reactivity, and thermal stability of the resulting porous structure. The resultant metal oxide-pillared layered titanates possess highly efficient CO_2 adsorption capability, which is greater than those of many other absorbents and compatible to those of CO_2 adsorbing MOF materials. The obtained pillared materials boast excellent thermal stability. This renders the present metal oxide-pillared layered titanates very promising CO_2 adsorbents. To the best of our knowledge, this is the first example of efficient CO_2 adsorbent from pillared materials. Because the co-pillaring of two kinds of inorganic nanoclusters is readily applicable for other nanosheets of layered inorganic solids, this method provides a facile way of developing new type of highly efficient CO_2 adsorbents.

4. Experimental Section

Sample Preparation: The host cesium titanate, $Cs_{0.67}Ti_{1.83-0.17}O_4$, was prepared by heating a stoichiometric mixture of Cs_2CO_3 and TiO_2.[48]

Its protonated derivative, $H_{0.67}Ti_{1.83-0.17}O_4 \cdot H_2O$, was obtained by the subsequent HCl treatment at room temperature for more than 3 days. The HCl solution was replaced with a fresh solution for at least 3 times. The exfoliation of the layered titanate could be achieved by reacting the protonated titanate with tetrabutylammonium hydroxide, or TBA·OH.[49] The hybridization between layered titanate nanosheets and chromium/cadmium oxides was carried out by the dropwise addition of the aqueous mixed solution (20 mL, 0.25 M, pH = 4.5) of chromium(III) acetate and cadmium(II) acetate into the colloidal suspension of exfoliated titanium oxide nanosheets (100 mL, 0.1 g L^{-1}, pH ≥ 12) under vigorous stirring.[21,26] The ratio of Cd/Cr was varied from 1/9 to 4/6 to probe the effect of chemical composition on the crystal structure and gas adsorption function of the pillared materials. After the mixing of two solutions, the cationic guest species were immediately flocculated with negatively charged titanate nanosheets. The reaction was performed under the reflux condition at 60 °C for 5 days. The resultant products were centrifuged, washed thoroughly with distilled water to remove excess ions, and dried in oven overnight.

Sample Characterization: The crystal structure of the pillared nanohybrids was determined by powder XRD (Rigaku, λ = 1.5418 Å, 25 °C). The chemical compositions and thermal behaviors of the nanohybrids were estimated by performing inductively coupled plasma spectrometry, or ICP, (Shimazu ICPS-5000), elemental CHN analysis (CE-Instruments-EA-1110), and thermogravimetric analysis (TGA) (Rigaku TAS-100), respectively. The crystallite morphology of the present samples was examined by FE-SEM using a JEOL JSM-6700F microscope. The stacking and in-plane structures of the nanohybrids were probed by performing HR-TEM or selected area electron diffraction (SAED) measurements with a JEOL JEM-2100F microscope at an accelerating voltage of 200 kV. To obtain cross-sectional images of the heterostructure, the nanohybrid sample was blended with acrylic resin (methyl methacrylate:*n*-butyl methacrylate = 4:6, 1.5% benzoyl peroxide) in a polyethylene capsule and then the sample was sliced using the ultramicrotome with a diamond knife. Additionally, energy dispersive spectrometry (EDS) analysis was done with a JEOL JSM-6700F microscope equipped with an energy dispersive X-ray spectrometer. X-ray absorption spectroscopy (XAS) experiments were carried out at the Ti K-edge, Cr K-edge, and Cd K-edge with the extended X-ray absorption fine structure (EXAFS) facility installed at the beam line 7C at the Pohang Accelerator Laboratory, or PAL, in Korea. The present XAS data were collected from the thin layer of powder samples deposited on transparent adhesive tapes in a transmission mode using gas-ionization detectors. The measurements were carried out at room temperature with a Si(111) single crystal monochromator. No focusing mirror was used. All the present spectra were carefully calibrated by measuring Ti, Cr, or Cd metal foil simultaneously.[50] The surface area and pore structure of the present nanohybrids were examined by measuring volumetrically nitrogen adsorption–desorption isotherms at liquid nitrogen temperature (–196 °C) with ASAP 2020 adsorption analyzer. The adsorption experiments of CO_2 and H_2 gases were performed at 0, 25, and –196 °C using the same adsorption analyzer, respectively. Before the adsorption measurement, all the present materials were degassed at 150 °C for 5 h under vacuum. The reproducibility of the CO_2 adsorption capacity of the nanohybrid was tested at 0 and 25 °C with the repeated CO_2 adsorption–desorption isotherm measurements.

Acknowledgements

T.W.K. and I.Y.K. contributed equally to this work. This research is supported by the Core Technology of Materials Research and Development Program of the Korea Ministry of Intelligence and Economy (grant No. 10041232), and by Korea Ministry of Environment(MOE) as "Converging Technology Program" (2012-000600003), and by National Research Foundation of Korea Grant funded by the Korean Government (2010-0001485). The experiments at PAL were supported in part by MOST and POSTECH.

Received: January 8, 2013
Published online: April 8, 2013

[1] C. Liu, U. Burghaus, F. Besenbacher, Z. L. Wang, *ACS Nano* **2010**, *4*, 5517.
[2] R. E. Morris, P. S. Wheatley, *Angew. Chem. Int. Ed.* **2008**, *47*, 4966.
[3] J. Lan, D. Cao, W. Wang, B. Smit, *ACS Nano* **2010**, *4*, 4225.
[4] N. A. Brunelli, S. A. Dias, K. Venkatasubbaiah, C. W. Jones, *J. Am. Chem. Soc.* **2012**, *134*, 13950.
[5] H. Kim, Y. Kim, M. Yoon, S. Lim, S. M. Park, G. S. Kim, K. Kim, *J. Am. Chem. Soc.* **2010**, *132*, 12200.
[6] F. Salles, H. Jobic, T. Devic, P. L. Llewellyn, C. Serre, G. Ferey, G. Maurin, *ACS Nano* **2010**, *4*, 143.
[7] S. Choi, J. H. Drese, C. W. Jones, *ChemSusChem* **2009**, *2*, 796.
[8] S. Zulfiqar, F. Karadas, J. Park, E. Deniz, G. D. Stucky, Y. Jung, *Energy Environ. Sci.* **2011**, *4*, 4528.
[9] T. M. McDonald, W. R. Lee, J. A. Mason, B. M. Wiers, C. S. Hong, J. R. Long, *J. Am. Chem. Soc.* **2012**, *134*, 7056.
[10] S. Ma, H.-C. Zhou, *Chem. Commun.* **2010**, *46*, 44.
[11] S. T. Meek, J. A. Greathouse, M. D. Allendorf, *Adv. Mater.* **2011**, *23*, 249.
[12] W. Kim, X. Zhang, J. S. Lee, M. Tsapatisis, S. Nair, *ACS Nano* **2012**, *6*, 9978.
[13] A. Zukal, I. Dominguez, J. Mayerová, J. Čejka, *Langmuir* **2009**, *25*, 10314.
[14] P. Yang, *The Chemistry of Nanostructured Materials*, World Scientific Publishing Co. Pte. Ltd., Singapore **2003**, pp. 1.
[15] A. Gil, R. Truhillano, M. A. Vicente, S. A. Korili, *Stud. Surf. Sci. Catal.* **2007**, *160*, 327.
[16] L. A. G. Aylmore, *Clays Clay Miner.* **1977**, *25*, 148.
[17] A. Gil, R. Truhillano, M. A. Vicente, in *Pillared Clays and Related Catalysts*, (Ed: A. Gil, R. Truhillano, M. A. Vicente), Springer, New York **2010**, pp. 23.
[18] J. L. Valverde, P. Canizares, M. R. S. Kou, C. B. Molina, *Clays Clay Miner.* **2000**, *48*, 424.
[19] E. Brunet, H. M. H. Alhendawi, C. Cerro, M. J. D. L. Mata, O. Juanes, J. C. Rodŕguez-Ubis, *Angew. Chem. Int. Ed.* **2006**, *45*, 6918.
[20] E.-J. Oh, T. W. Kim, K. M. Lee, M.-S. Song, A.-Y. Jee, S. T. Lim, H.-W. Ha, M. Lee, J.-H. Choy, S.-J. Hwang, *ACS Nano* **2010**, *4*, 4437.
[21] T. W. Kim, S. G. Hur, S.-J. Hwang, H. Park, W. Choi, J.-H. Choy, *Adv. Funct. Mater.* **2007**, *17*, 307.
[22] T. W. Kim, S.-J. Hwang, S. H. Jhung, J.-S. Chang, H. Park, W. Choi, J.-H. Choy, *Adv. Mater.* **2008**, *20*, 539.
[23] H. N. Kim, T. W. Kim, I. Y. Kim, S.-J. Hwang, *Adv. Funct. Mater.* **2011**, *21*, 3111.
[24] R. T. Yang, *Adsorbents: Fundamentals and Applications*, Wiley, New York **2003**.
[25] K. M. Thomas, *Catal. Today* **2007**, *120*, 389.
[26] C. F. Baes Jr., R. E. Mesmer, *The Hydrolysis of Cations*, John Wiley & Sons, New York **1982**, pp. 295.
[27] J.-H. Choy, J.-H. Park, J.-H. Yang, *J. Phys. Chem. B* **1998**, *102*, 5991.
[28] K. Fukuda, I. Nakai, C. Oishi, M. Nomura, M. Harada, Y. Ebina, T. Sasaki, *J. Phys. Chem. B* **2004**, *108*, 13088.
[29] J. L. Gunjakar, T. W. Kim, H. N. Kim, I. Y. Kim, S. -J. Hwang, *J. Am. Chem. Soc.* **2011**, *133*, 14998.
[30] S.-J. Hwang, J.-H. Choy, *J. Phys. Chem. B* **2003**, *107*, 5791.
[31] T. Allen, *Particle Size Measurement*, 4th ed., Chapman and Hall, London **1980**.
[32] Y.-M. Jeon, G. S. Armatas, J. Heo, M. G. Kanatzidis, C. A. Mirkin, *Adv. Mater.* **2008**, *20*, 2105.
[33] H. J. Lee, W. Cho, S. Jung, M. Oh, *Adv. Mater.* **2009**, *21*, 674.
[34] A. Gil, R. Trujillano, M. A. Vicente, S. A. Korili, *Int. J. Hydrogen Energy* **2009**, *34*, 8611.
[35] X. Lin, A. J. Blake, C. Wilson, X. Z. Sun, N. R. Champness, M. W. George, P. Hubberstey, R. Mokaya, M. Schröder, *J. Am. Chem. Soc.* **2006**, *128*, 10745.

[36] Y.-G. Lee, H. R. Moon, Y. E. Cheon, M. P. Suh, *Angew. Chem. Int. Ed.* **2008**, *47*, 7741.
[37] M. Sevilla, R. Mokaya, A. B. Fuertes, *Energy Environ. Sci.* **2011**, *4*, 2930.
[38] R. G. Pearson, *J. Am. Chem. Soc.* **1963**, *85*, 3533.
[39] D. W. Smith, *J. Chem. Educ.* **1987**, *64*, 480.
[40] D. Bonenfant, M. Kharoune, P. Niquette, M. Mimeault, R. Hausler, *Sci. Technol. Adv. Mater.* **2008**, *9*, 013007.
[41] P. Pachfule, T. Panda, C. Dey, R. Banerjee, *CrystEngComm.* **2010**, *12*, 2381.
[42] P. Pachfule, Y. Chen, J. Jiang, R. Banerjee, *J. Mater. Chem.* **2011**, *21*, 17737.
[43] S. Ma, *Pure Appl. Chem.* **2009**, *81*, 2235.
[44] P. Ryan, L. J. Broadbelt, R. Q. Snurr, *Chem. Commun.* **2008**, 4132.
[45] O. K. Farha, A. O. Yazaydın, I. Eryazici, C. D. Malliakas, B. G. Hauser, M. G. Kanatzidis, S. T. Nguyen, R. Q. Snurr, J. T. Hupp, *Nat. Chem.* **2010**, *2*, 944.
[46] S. Cui, W. Cheng, X. Shen, M. Fan, A. T. Russell, Z. Wu, X. Yi, *Energy Environ. Sci.* **2011**, *4*, 2070.
[47] Z. Z. Yang, L. N. He, Y. N. Zhao, B. Li, B. Yu, *Energy Environ. Sci.* **2011**, *4*, 3971.
[48] I. E. Grey, C. Li, I. C. Madsen, J. A. Watts, *J. Solid State Chem.* **1987**, *66*, 7.
[49] T. Sasaki, M. Watanabe, *J. Am. Chem. Soc.* **1998**, *120*, 4682.
[50] B.-K. Teo, *EXAFS: Basic Principles and Data Analysis*, Springer Verlag, Berlin **1986**.